IEEE Access
Multidisciplinary | Rapid Review | Open Access Journal

IEEE POWER & ENERGY SOCIETY SECTION

Received 27 April 2023, accepted 19 May 2023, date of publication 20 June 2023, date of current version 26 June 2023.

Digital Object Identifier 10.1109/ACCESS.2023.3288023

RESEARCH ARTICLE

Innovative Microstepping Motor Controller With Excitation Angle-Current Dual-Loop Feedback Control

SHYH-BIAU JIANG, (Member, IEEE), HSIANG-CHUN CHUANG, CHUNG-WEI KUNG, XIANG-GUAN DENG, YEN-PING SHEN, AND LI-WU CHEN

Institute of Opto-Mechatronics Engineering, National Central University, Taoyuan City 32001, Taiwan

Corresponding author: Hsiang-Chun Chuang (x210465@hotmail.com)

This work was supported by Roboy Venture Capital Company Ltd., which is a venture capital company in Taiwan, it provides funds to help the researchers to realize the research if the researchers have innovative research ideas. The finance support includes the personnel fees of research, materials of research, and publishing fees of paper.

ABSTRACT In this paper, an innovative control method, namely angle-current dual-loop feedback control, is proposed for use with microstepping motors. This method involves adjusting the stator excitation angle and current simultaneously on the basis of the feedback angle of the sensor on the microstepping motor. The proposed method is expected to enhance the positioning accuracy and energy efficiency of stepping motors. The proposed method was tested by implementing it in a microstepping motor control system, which included a core microcontroller unit circuit, dual-H-bridge pulse width modulation drive circuit, current sensing circuit, and angle sensing encoder readback circuit. An algorithm based on the proposed method was developed, and data sampling, storage, and return communication functions, which are convenient for experimental verification, were included in this algorithm. To verify that the proposed method is superior to traditional open-loop control and excitation angle feedback control, a testing platform was used to measure the differences in positioning accuracy and drive power under the three control methods and biased torsion loads. The results indicate that compared with the other two control methods, the proposed control method improves the positioning accuracy and reduces the power consumption of a stepping motor.

INDEX TERMS Angle control, current control, dual loop, positioning accuracy, power efficiency, stepping motor.

I. INTRODUCTION

In this paper, an innovative control method, namely angle–current dual-loop (ACDL) feedback control, is proposed for microstepping motors. In this method, the stator excitation angle and current are adjusted simultaneously on the basis of the sensor angle of a microstepping motor. The proposed method is expected to improve the positioning accuracy and energy efficiency of microstepping motors.

The machining precision achieved by a company is a key indicator of its technological capabilities. For example, in integrated-circuit manufacturing, the machining precision indicates the maturity of the machining process, with precision values of 28 and 3 nm indicating a mature process and high-end process, respectively. Before the Industrial Revolution, precision manufacturing ability was mainly determined by the technical literacy of craftspeople. Since the Industrial Revolution, the precision manufacturing ability has been determined by the resolution of precision machinery for the positioning of cutting tools. The main power source of modern machinery is the motor, and the control of simple mechanical actions can be achieved only by starting and stopping the motor. However, precision machining also requires control of the accuracy of the angle and speed of the motor. Sensing elements, such as encoders and tachometers, are used to sense the angle or speed, and controlling the motor to reach the required position or speed is called speed or positioning servo control, respectively. The core device involved in precision machining is a positioning servo.

In servo motors, a permanent magnet synchronous motor is usually used as a rotary actuator [1], and an angle encoder

The associate editor coordinating the review of this manuscript and approving it for publication was Kaushik Mukherjee.

is employed to measure the feedback angle. A servo motor composed of these two components performs highly in speed servo control [2]. However, it often vibrates at the final positioning point during positioning control [3], which limits the positioning precision. For machines with low torque loads and high positioning accuracy requirements, stepping motors are usually used rather than servo motors. The commonly used two-phase stepping motor has a positioning resolution limit of 1.8° [3], whereas the less commonly used five-phase stepping motor has positioning resolution of 0.72° [3], [4]. Although an open-loop microstepping drive control method does exist, the resolution of the stator output magnetic field vector can be improved through subdivision of the magnetic field vector, and the angular resolution can be improved. However, because of the influences of motor manufacturing variation [5] and rotor cogging torque [6], [7], the subdivision of the rotor angle corresponding to the stator vector is not uniform. Therefore, the angular precision of the open-loop microstepping drive control method cannot meet the angular resolution requirements, and accurate positioning cannot be guaranteed. In addition, the method used for driving a stepping motor involves switching the magnetization phase of the stator so that the static balance point of the rotor moves with the magnetization phase, and the rotor is induced to rotate. Because this method can provide stable holding torque, the rotor can remain stationary at the static equilibrium point and achieve better positioning performance than a traditional servo motor. However, when the motor is static, it does no work but maintains the drive current and dissipates power in the coil resistance, which not only reduces the driving efficiency but also causes the motor to heat up [8].

The rotation of the motor pulls the rotor through the change in the magnetic field of the stator. On the basis of the angular difference between the magnetic fields of the stator and rotor, the stator generates two-phase (phase d and q) traction forces that act on the rotor. Phase d provides holding torque, whereas phase q provides motor rotation torque [9]. The control method for a traditional servo motor involves sensing the rotor's position, controlling the phase-d current of the stator to be 0, and controlling the phase-q current of the stator to generate torque for controlling the rotation [10]. When the positioning error is close to 0, the phase-q torque generated for feedback control by the error in the reference rotor angle exerts a pushing force on the rotor to reduce the positioning error at the beginning of each sampling period; however, after the rotor crosses the balance point and before the end of the control cycle, the phase-q torque maintains the same direction and pushes the rotor away from the balance point until the end of the control cycle even though the direction of the error has been reversed. Therefore, when a traditional servo motor is positioned, the rotor vibrates at the target point and cannot stop at this point.

In the traditional stepping motor drive method, the target balance position of the rotor is referred to, and the stator is controlled to provide the phase-d current at the target position. Because the rotor does not stop until it reaches the target balance position, the motor rotates to the target angle. For a two-phase stepping motor, the balance position of each electronic cycle is A, B, $\bar{A}$, and $\bar{B}$ in sequence; thus, when switching the current in accordance with this phase sequence, the motor rotates at an electronic angle of 90° per step [3]. The step resolution can be improved using the microstep driving method to adjust the excitation current ratio of adjacent two-phase coils to improve the resolution of the stator magnetic field vector [11], [12], [13]. The advantage of using the stepping drive method for positioning is that when the rotor deviates from the balance point, the stator generates holding torque proportional to the deviation angle and pulls the rotor back to the balance point. However, if the machine driven by the stepping motor is subjected to biased load torque, the rotor must deviate to a sufficiently high angle to offset the biased load torque for balancing the torque; thus, the positioning accuracy of a stepping motor is strongly affected by a biased load.

Positioning errors are usually eliminated using encoder feedback. Reference [14] proposed a new position control method using a low-resolution encoder, using the least squares method to fit the position data from the Hall position sensor to derive a high-resolution rotor position predictor, which can effectively improve the positioning stability. Several studies have mentioned that using an encoder to measure the rotor angle can eliminate open-loop positioning errors. Reference [15] developed a closed-loop control system consisting of a microcontroller, a hybrid stepper motor, a driver, and an encoder. Reference [16] uses a low-cost magnetic rotary position sensor and vector control for positioning, with a maximum error of 1.19°. Reference [17] Perform current/speed/position closed-loop control on stepper motors, evaluate classic PI regulators, sliding mode control, deadbeat predictive current control, and model predictive current control. PI control performs better at low current. Reference [18] control the stepper motor in a closed loop, and the methods include current control, position control, and damping control. The improved PI current control is adopted to ensure the current tracking performance and increase the speed response bandwidth. This method of feedback control the excitation angle between the stator and the rotor is referred to as excitation angle loop (AL) control. This feedback-driving method results in the simultaneous generation of phase-d and phase-q currents. The phase-d current is beneficial for generating holding torque, whereas the phase-q current resists a biased load. However, because the driving current of the driving method is fixed at the rated value, it still consumes considerable power. An innovative driving method called ACDL feedback control is proposed in this paper. This method combines the advantages of conventional servo motor control and microstepping driving, with a balance being achieved between positioning accuracy and power efficiency. In addition to the feedback control of the excitation angle of the stator, the total current is controlled on the basis of error feedback in the proposed method. When the excitation angle is small, the excitation angle

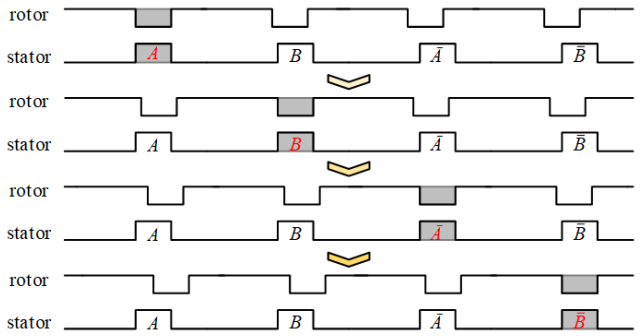

FIGURE 1. Timing sequence diagram of a stepping motor driven in the full-step mode.

feedback loop dominates, and holding torque is generated with the lowest phase-d current, which avoids the positioning vibration caused by phase-q current. When the angular error is large, the excitation angle is saturated and fixed at ±90°. At this time, the system is dominated by current feedback control, and phase-q current provides the maximum torque under the rated current to resist the biased load so that the highest power efficiency is achieved.

II. STEPPING MOTOR STRUCTURE AND DRIVING ALGORITHM

Depending on their stator type, stepping motors can be classified into three types: variable-reluctance-type, permanent-magnet-type, and hybrid-type stepping motors [19]. Depending on the number of coil phases, stepping motors can be classified into four types: two-, three-, four-, and five-phase stepping motors [20]. The basic structure of two- and four-phase stepping motors is the same; the difference between them lies in whether they distinguish positive and negative phases of the coil. The mechanical structure of a permanent-magnet-type stepping motor is composed of coaxial electromagnets and multiple sets of N–S permanent magnets. Because of the limited space occupied by the magnetized coil, the density of the permanent magnetic poles cannot be increased easily; thus, the stepping resolution is low. The hybrid-type stepping motor splits the coil core to increase the cog, thereby increasing the step angle resolution.

The timing sequence diagram of a stepping motor driven in the full-step mode is shown in Fig. 1. In this figure, the upper flange represents the rotor cog; the lower flange represents the electromagnet of the stator; and A, B, $\bar{A}$, and $\bar{B}$ denote different excitation coils. The figure indicates the positions of four rotors relative to the corresponding stators (i.e., the four sequences of phases A, B, $\bar{A}$, and $\bar{B}$). As displayed in Fig. 1, the stable rotor position under stator excitation is different for each phase. As the stator switches the excitation phase in the time sequence, the stable position of the rotor gradually moves from left to right and then drives the rotor to rotate. However, irrespective of whether a permanent-magnet-type or hybrid-type stepping motor is used, the rotor vibrates during rotation because its driving method involves

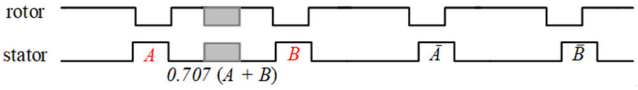

FIGURE 2. Diagram of a stepping motor driven in half-step intervals.

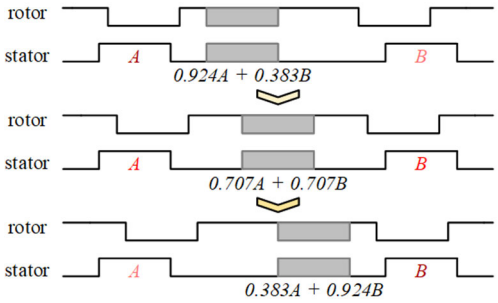

FIGURE 3. Timing diagram of a stepping motor driven by 1/4 steps.

phase switching to make the rotor move between different stable angles [21]. This vibration is especially obvious at low rotation speed [22], [23].

Fig. 2 displays a schematic of a half-step drive of a stepping motor. Consider phases A and B as an example. Ensuring the simultaneous excitation of phases A and B between the separate excitations of these phases is equivalent to adding a stable phase with a half-step interval between these phases. This process can increase the resolution of driving the stepping motor, decrease the jump interval caused by switching phases of stepping, and reduce the jump impact. In Fig. 2, the upper and lower gray flanges represent the equivalent cog slots of the rotor and the equivalent phase-A–B excitation coils of the stator, respectively. The position of the rotor when the equivalent cog slot of the rotor is aligned with the equivalent phase-A–B excitation coil is the stable position of the newly inserted half-step interval.

Not confined to half-stepping, the same microsegmentation concept can insert three 1/4 steps, seven 1/8 steps, or higher-resolution microstepping between two phases [24]. Fig. 3 depicts the timing diagram for a stepping motor driven by 1/4 steps. Three equivalent cogs of 0.924A + 0.838B, 0.707A + 0.707B, and 0.838A + 0.924B are inserted between the cogs of phases A and B to obtain a resolution of 1/4 step per stepping.

Although the stepping motor vibrates because of the jumping between phases when it rotates, as it reaches the equilibrium point and enters a steady state, it remains stationary under the influence of the holding torque generated by the phase-d excitation.

Fig. 4 displays a diagram of the cogging and magnetic pole moment vectors. The upper flange is the equivalent cogging of the rotor, and the lower flange is the equivalent excitation pole of the stator. As indicated by the dashed-line equivalent cog, when the center of the cog is aligned with the center of the magnetic pole, there is only a magnetic force vector parallel to the line connecting the two center points, which

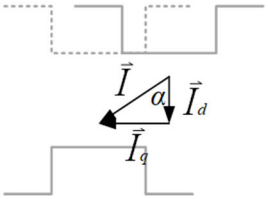

FIGURE 4. Diagram of the cogging and magnetic pole moment vectors.

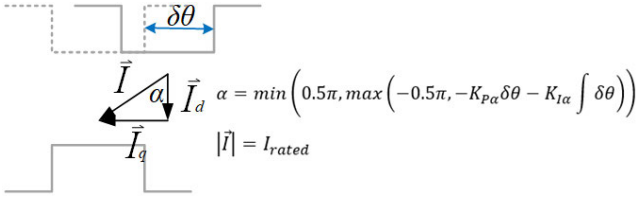

FIGURE 5. Schematic diagram of the excitation angle PI loop control, AL.

represents the direct magnetic force, that is, the phase-d magnetic force. As suggested by the solid-line equivalent cog, when an angular difference exists between the equivalent cog and the equivalent magnetic pole, in addition to the phase-d magnetic force, a phase-q magnetic force exists perpendicular to the phase-d magnetic force. Because of the limitation of the motor structure, the rotor can only move in a direction parallel to the phase-q magnetic force. Therefore, the phase-d magnetic force is perpendicular to the rotation direction and cannot push the rotor to perform work; only the phase-q magnetic force can make the motor rotate. The excitation angle α is defined as the angle between the composite vector of q and d and the phase vector of d. When the equivalent cog and equivalent magnetic pole are aligned, α is 0, which represents the equilibrium position of the rotor. Suppose the equivalent cog deviates from the equivalent magnetic pole. In this case, phase-q torque, namely the holding torque, exists opposite to the deviation of the equivalent cog direction and resists the cog offset. The greater the deviation, the higher α and the holding torque. When the excitation current is fixed, the holding torque increases with the cosine function of α. Until α reaches $\pm 0.5\pi$, the phase-q torque and driving efficiency reach their maximum values. When the absolute value of α exceeds 0.5π, the holding torque decreases, it may be unable to balance the load torque and thus be out of step of the motor.

Fig. 5 presents a diagram of excitation angle proportional–integral (PI) loop control. In this figure, the upper solid-line flanges represent the current equivalent cogging position of the rotor, the upper dotted-line flange indicates the target equivalent cogging position, and $\delta\theta$ indicates the angular error between these positions. The lower solid-line flange represents the equivalent magnetic pole of the stator. The excitation angle PI loop controller is hereafter referred to as the AL controller. The AL controller senses the angle of the rotor, calculates the angular error, and uses PI feedback to

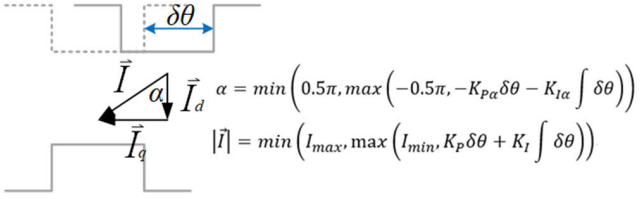

FIGURE 6. Diagram of ACDL feedback control.

adjust the excitation angle α, as expressed in (1).

$$\alpha = \min\left(0.5\pi, \max\left(-0.5\pi, -K_{\mathrm{P}\alpha}\delta\theta - K_{\mathrm{I}\alpha}\int \delta\theta\right)\right) \tag{1}$$

Because the cosine function reaches its extreme value at $\pm 1/2\pi$, $1/2\pi$ is the limit of the absolute α value. The total excitation current is fixed at the rated current; thus, $\left|\vec{I}\right| = I_{\mathrm{rated}}$.

When the angular error is 0, the total current only contains the phase-d current component, which provides the holding torque. When the angular error is positive, α is negative and phase-q has a negative current component, which can reduce the error. The greater the error, the higher the negative value of α, the larger the phase-q component $I_{\mathrm{rated}} \times \cos\alpha$, and the smaller the phase-d component $I_{\mathrm{rated}} \times \sin\alpha$. When the absolute value of α reaches $1/2\pi$, the phase-d current component reaches its maximum value. A further increase in α only causes a reduction in the phase-q current; thus, $1/2\pi$ and $-1/2\pi$ are the upper and lower limits of α, respectively. The AL controller provides excellent holding torque at the rated current; however, when the angular error is not 0, the supplied phase-d current consumes the energy without benefit.

Fig. 6 displays a diagram of the proposed ACDL feedback control method. In addition to the excitation angle loop of the AL controller, the ACDL controller contains a total current control loop, as expressed in (2).

$$\left|\vec{I}\right| = \min\left(I_{\mathrm{max}}, \max\left(I_{\mathrm{min}}, K_{\mathrm{P}}\delta\theta + K_{\mathrm{I}}\int \delta\theta\right)\right) \tag{2}$$

The total current control loop controls the total current output in accordance with the negative feedback and integral value of the angular error. To maintain the static holding torque of the stepping drive, a minimum limit is set for the output current, and an upper limit is set for the total current in accordance with the maximum allowable current limit of the motor.

When the angular error is small, the PI feedback current is smaller than the lower limit of the output current. The PI feedback current is then set as the lower limit of the output current. At this time, the ACDL controller can be simplified to an AL controller, and the output lower-limit current provides the holding torque. When the angular error is high, the PI feedback value of the excitation angle exceeds the upper limit and is fixed as saturation value $\pm 1/2\pi$. At this time,

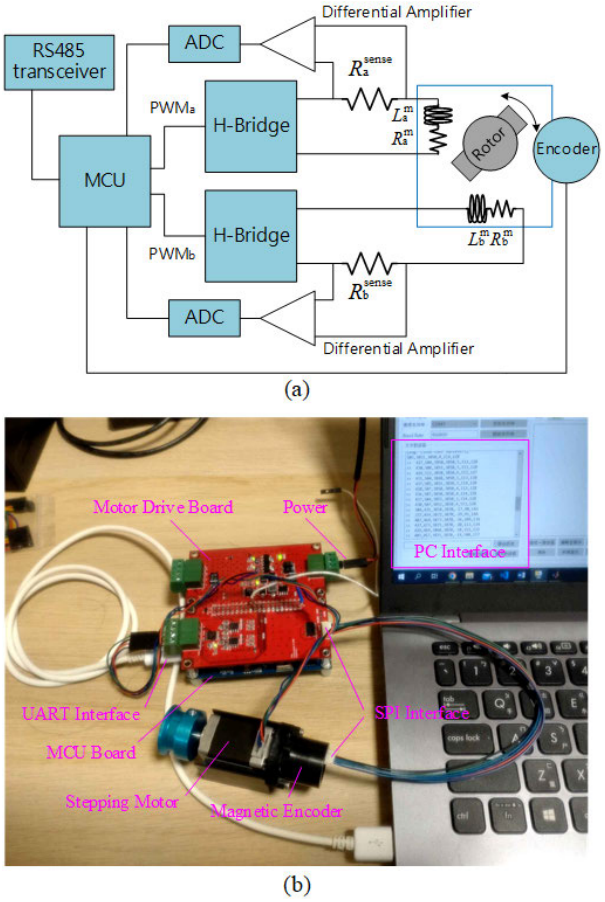

FIGURE 7. (a) Circuit diagram and (b) photograph of the constructed stepping motor drive.

the ACDL controller can be simplified to a phase-q-current PI negative feedback controller and provides high-energy-efficiency driving torque. Compared with the AL controller, the ACDL controller has lower holding torque and possibly lower positioning accuracy but considerably higher power efficiency.

III. DESIGN OF STEPPING MOTOR DRIVE SYSTEM

To evaluate and compare the benefits of traditional microstepping, AL control, and ACDL control, we constructed a stepping motor drive system, installed the system with an algorithm based on the proposed control method, and conducted experiments to measure the efficiency and performance of various control algorithms. As depicted in Fig. 7, the stepping motor drive circuit contained an ATMEGA M128 microcontroller unit (MCU), and the universal asynchronous receiver/transmitter (UART) port of this circuit was designed as an RS485 serial communication port so that the circuit could receive control commands from a computer and report experimental data. Two pulse width modulation (PWM) output ports of the MCU, namely PWMa and PWMb, were used to control a dual-H-bridge drive circuit. The two H-bridges drove the phase-A and phase-B coils of the two-phase stepping motor, respectively. Each of these coils was

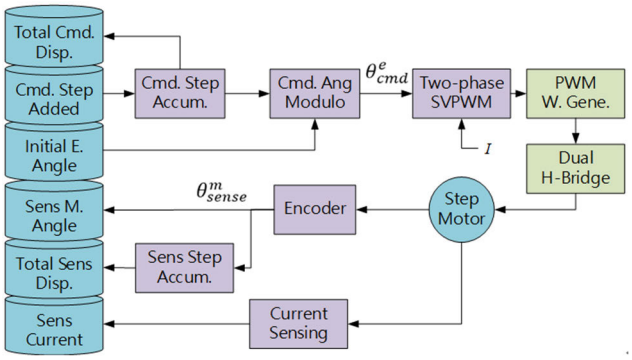

FIGURE 8. Functional block diagram of a traditional open-loop microstepping driver.

connected in series with a current sensing resistor, and a differential amplifier was used to amplify the voltage across the resistors and feed it to the analog-to-digital converter (ADC) port of the MCU so that the MCU could read the current of the two phases. A 14-bit AS5047D angle encoder with a theoretical resolution of 0.022° was installed on one of the output shafts of the dual-output shaft stepping motor to measure the rotor position of the stepping motor. The encoder contained a serial peripheral interface (SPI) serial communication port, and the MCU could read back the absolute position of the stepping motor through SPI. The circuit diagram and a photograph of the constructed stepping motor drive circuit are displayed in Fig. 7(a) and 7(b), respectively.

The same circuit board, through programming three different programs, was used to perform traditional microstepping control, AL control (single-closed-loop control), and ACDL control. The functional blocks of the algorithms in the various control methods are described in the following text.

Fig. 8 displays the functional block diagram of a traditional open-loop microstepping driver. Command step added refers to the value-added step command from the monitoring computer, which is fed into the command step accumulator to produce the angular displacement command. The obtained result is then fed into the command angle modulo operator and divided by the number of steps per circle to obtain the remainder, which is the electronic angle command θ^{e}_{cmd}. The electronic angle command is fed into the two-phase space vector PWM (SVPWM) to calculate the PWM commands for the cosine wave of phase A and the sine wave of phase B. Moreover, the rated current I is used to calculate the two sinusoidal waves. The PWM command is written into the output value register of the peripheral hardware (PWM wave generator) of the MCU, which results in the generation of a two-phase PWM output wave. The two-phase PWM output wave controls the dual-H-bridge power amplifier circuit to provide sine- and cosine-wave voltages across the two-phase coil of the stepping motor. The coil current generated by the two-phase cross-voltage drives the stepping motor to rotate, and is then measured by the current sensing circuit. The angle encoder reads the angle of the motor rotor,

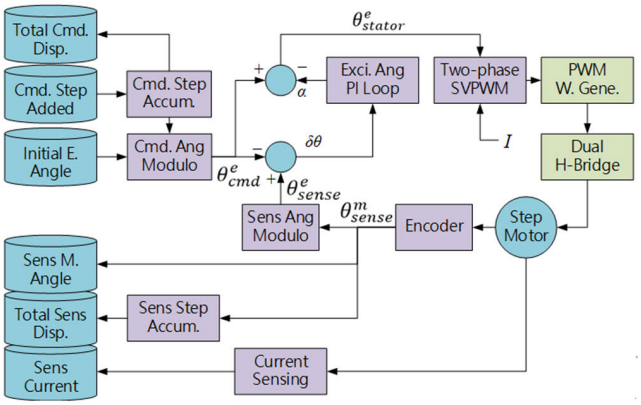

FIGURE 9. Functional block diagram of an AL microstepping driver.

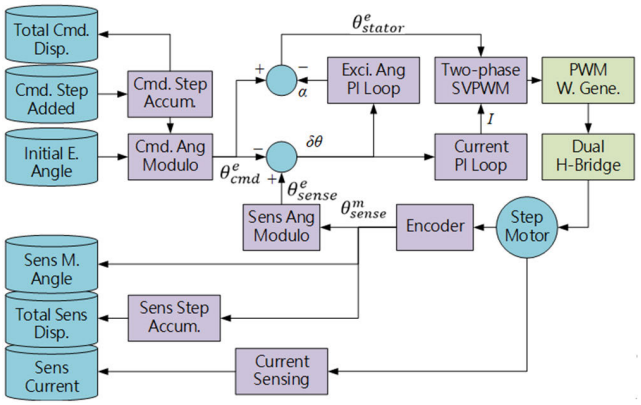

FIGURE 10. Functional block diagram of an ACDL microstepping driver.

which is the sensed mechanical angle $\theta^{\mathrm{m}}_{\mathrm{sense}}$. The sensed step accumulator accumulates the values of the sensed mechanical angle to calculate the total sensed displacement. In addition to providing the command step added function through RS485 communication, the monitoring computer can set the initial electronic angle at the beginning of the experiment. Moreover, it can read back the total command displacement, sensed mechanical angle, total sensed displacement, and sensed currents, all of which are used to calculate motor positioning accuracy and power consumption.

Fig. 9 depicts the functional block diagram of an AL microstepping driver. The stator angle $\theta^{\mathrm{e}}_{\mathrm{stator}}$ is controlled by the excitation angle PI loop, in addition to the open-loop rotor command angle $\theta^{\mathrm{e}}_{\mathrm{cmd}}$, additionally adds excitation angle α. The encoder senses the mechanical angle $\theta^{\mathrm{m}}_{\mathrm{sense}}$ of the motor and calculates the sensed electronic angle $\theta^{\mathrm{e}}_{\mathrm{sense}}$ through the sensed angle modulo operator. The sensed electronic angle $\theta^{\mathrm{e}}_{\mathrm{sense}}$ is subtracted from the command electronic angle $\theta^{\mathrm{e}}_{\mathrm{cmd}}$ to calculate the electronic angle control error $\delta\theta$, which is amplified through excitation angle PI loop feedback to obtain the excitation angle α. The rotor angle command $\theta^{\mathrm{e}}_{\mathrm{cmd}}$ is then used to correct the stator excitation position $\theta^{\mathrm{e}}_{\mathrm{stator}}$. The remaining functional blocks, commands, settings, and data collection steps of the AL microstepping driver are the same as those for the traditional open-loop microstepping driver.

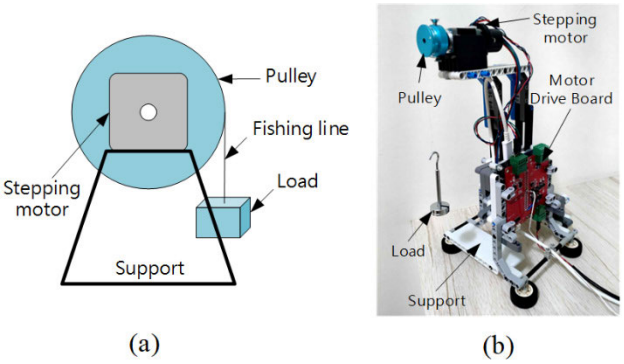

FIGURE 11. Experimental platform for biased load testing: (a) schematic and (b) photograph of the platform.

Fig. 10 depicts a functional block diagram of an ACDL microstepping driver. In contrast to AL control, ACDL control involves a current PI loop. The rotor angle error $\delta\theta$ is not only fed into the excitation angle PI loop to calculate the excitation angle α but also fed into the current PI loop to calculate the absolute feedback excitation current $|I|$. The parameter $|I|$ replaces the original fixed rated current and is fed into the two-phase SVPWM controller to control the voltage across the phase-A and phase-B coils. The remaining functional blocks, commands, settings, and data collection steps of the ACDL microstepping driver are the same as those of the AL microstepping driver.

IV. EXPERIMENTAL DESIGN

Because the positioning accuracy of the traditional microstepping motor drive method is easily affected by the biased load torque, we constructed a biased load test platform to test the performance of resists the biased load of the developed drive method of stepping motor.

Fig. 11 displays the configuration of the developed biased load test platform. The biased load was applied by installing a pulley on the output shaft of the stepping motor and hanging a counterweight from an almost weightless fishing line run over the pulley. The motor size was 20 mm × 20 mm × 34 mm, 200 steps per turn, the rated current was 0.6 A, the minimum limit current was set to 0.4 A, and the maximum output torque was 1.8 N-cm; the other specification of the motor [25], please refer to Table 1. The radius of the pulley was 1 cm; after a hole was drilled in the pulley, one end of the fishing line was passed through the hole and fixed to the pulley, and the other end was tied to a loop to mount a weight of 20 g, which provided torque load of 0.2 N-cm.

To evaluate and compare the effectiveness of traditional open-loop control, AL single-loop control, and ACDL dual-loop control, these three methods were used to perform 1, 1/2, 1/4, and 1/8 microstep positioning control on the developed test platform. The positioning accuracy and power consumption were examined under no load, forward-biased load, and reverse-biased load to compare the accuracy and power efficiency for the aforementioned methods. To compare the different control strategies, the rotation speed and control

TABLE 1. Motor specifications used in experiments.

Step Angle	1.8	Deg.
Current	0.6	A/Phase
Resistance	4.5	Ω/Phase
Inductance	1.2	mH/Phase
Holding Torque	1.8	N-cm
Length	34	mm
Inertia	1.9	10^{-7}Kg-m^2
Mass	0.06	kg

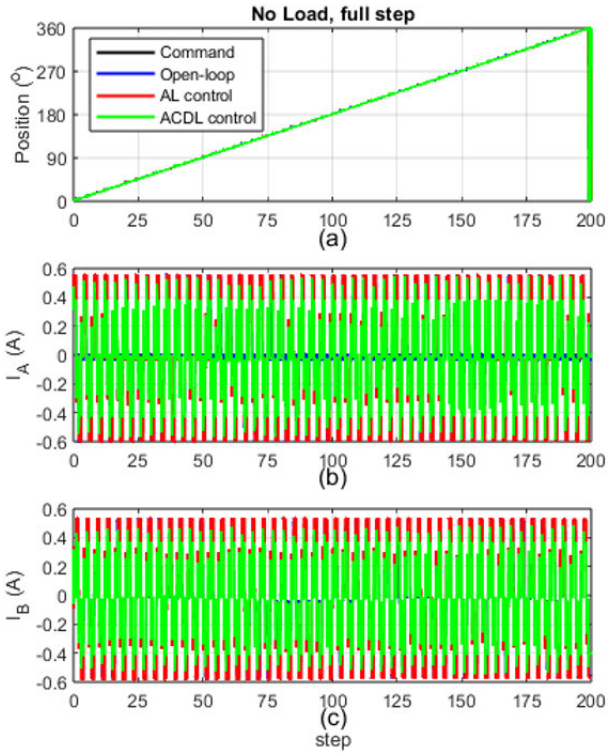

FIGURE 12. Original data obtained under the no-load condition and a full-step drive. The horizontal axis represents the number of command steps, and the vertical axis represents the (a) rotor angle, (b) phase-A current (A), and (c) phase-B current (A).

period of open-loop, AL, and ACDL control are the same in the experiment, where the time of AL control occupies 5% of the control period, and the ACDL control increases to 10% because of the addition of a current PI loop compared with AL control.

V. DATA OF DRIVE PERFORMANCE TEST

Fig. 12 displays the original data for the stepping motor when it completed one rotation under full-step control and no biased load. Fig. 12(a)–12(c) displays the rotor angle, phase-A current, and phase-B current, respectively, corresponding to the step command angle. The data in Fig. 12 indicate that under the three control methods, the angles followed the control command to complete a rotation, and the phase-A and phase-B currents completed 50 cycles, i.e., 200 steps. For the forward-biased loads, reverse-biased loads, and different microsteps, the original data looked similar, and

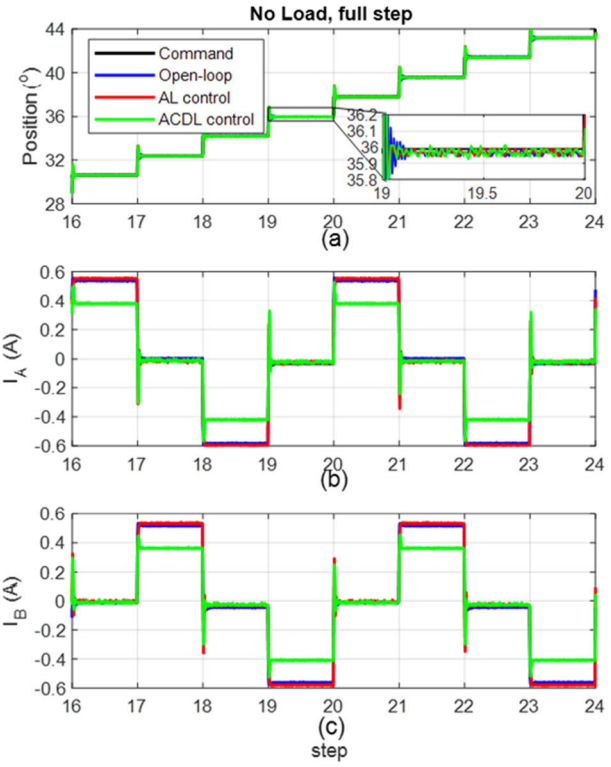

FIGURE 13. Data obtained under the no-load condition and a full-step drive for eight steps. (a) Rotor angle curves for the three control modes, with the lower-right corner displaying the zoomed-in data for a single step. Curves of the (b) phase-A and (c) phase-B currents under the three control modes. The blue, red, and green curves represent the currents under open-loop control, AL control, and ACDL control, respectively.

observing the details under the scale of this picture became difficult.

To improve the resolution of the horizontal axis, two electronic angular periods equivalent to eight steps in Fig. 12 were used to draw Fig. 13. In Fig. 13(a), the data for a single step are enlarged in the lower-right corner. In all three control methods, the rotor oscillated and converged to a steady state. The steady-state angle values of the rotor in the two feedback control methods were close to the command angle, whereas the steady states in the open-loop control method exhibited small but discernable errors. Theoretically, the full-step drive should have no angular deviation when no load is applied. The aforementioned steady-state error originated from a variation in the motor's manufacturing. In all three control methods, the transient overshoot phenomenon, which originates from the impact of the step command, was observed. Fig. 13(b) and 13(c) show the phase-A and phase-B currents, respectively, under the no-load condition and a full-step drive. The current under open-loop and AL control was fixed at the rated value of 0.6 A. Under ACDL control, because of the current PI feedback control, the current converged to a steady state after oscillating. The current surged to a maximum value of 0.6 A in the initial stage of phase switching and then converged to a preset lower limit of 0.4 A in the steady state.

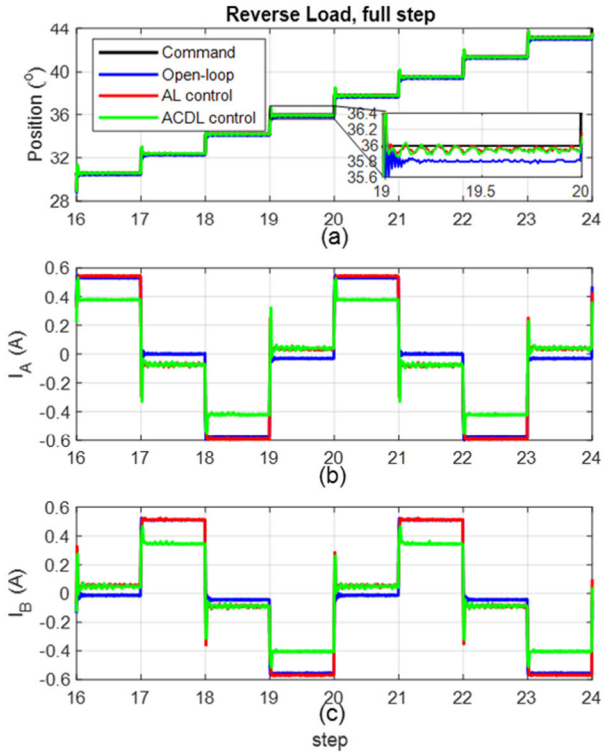

FIGURE 14. Data obtained under the reverse-load condition and a full-step drive for eight steps.

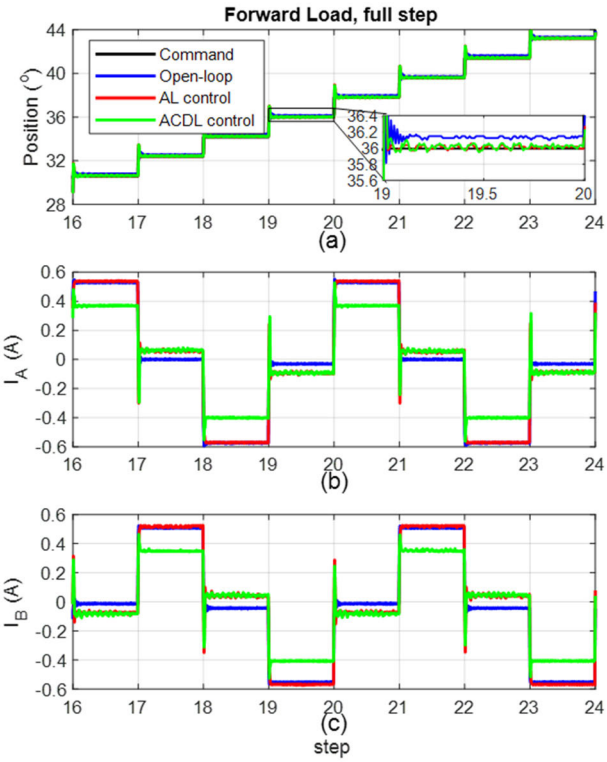

FIGURE 15. Data obtained under the forward-load condition and a full-step drive for eight steps.

Fig. 14 depicts the data measured under a reverse load and full-step drive for eight steps. Fig. 14(a) shows the rotor angle curve, the enlarged view of which indicates that the forward angle was marginally smaller than the required command under reverse load, with the error being greater under open-loop control (approximately $-0.2°$) than under the other two control methods. Fig. 14(b) and 14(c) display the curves of the phase-A and phase-B currents, respectively, under the aforementioned condition. The two-phase current controlled by the open loop switched between 0, the positive rated current, and the negative rated current, all of which were phase-d currents. In AL control and ACDL control, a value that should be 0 appears in the phase-q current to counterbalance the reverse load, and its sign was the same as the phase of the next step. The phase-q currents of the aforementioned two feedback control methods were consistent, which indicated that these methods produced the same phase-q current to resist certain reverse load. Because of the existence of phase-q current, the phase-d current in AL control was marginally reduced to maintain the scalar synthesized by the vectors of the currents of the two phases as the rated current. The phase-d current in ACDL control was smaller than that in AL control because the total current could be decreased in ACDL control. In both the aforementioned feedback control methods, the overshoot phenomenon was observed because of the surge in angular error in the initial stage of phase switching; however, in both methods, the current converged to a steady-state value quickly after the aforementioned phenomenon.

Fig. 15 displays the data obtained under the forward-load condition and a full-step drive for eight steps. Fig. 15(a) depicts the rotor angle curve obtained under the aforementioned conditions. The enlarged image in this figure indicates that the influence of the forward load caused the forward angle to be marginally higher than the required command, with the highest error being observed under open-loop control ($0.15°$). Fig. 15(b) and 15(c) depict the curves of the phase-A and phase-B currents, respectively, under the aforementioned conditions. Similar to the situation observed under reverse negative load, the two-phase current switched between 0, the positive rated current, and the negative rated current, all of which were phase-d currents, in the open-loop control method under forward load. The phase-q current also had a nonzero value in the AL and ACDL control methods; however, the sign of this current was opposite to that of the reverse load to resist the forward load. These two feedback control methods also generated the same phase-q current to resist certain forward load. As in the scenario under reverse load, under forward load, the phase-d current decreased, whereas the total current remained unchanged in the AL control method because of the sharing of the phase-q current. The phase-d current also decreased under ACDL control because of the reduction in the total current. In the AL and ACDL control methods, the phenomenon of convergence to a steady state was observed after overshooting.

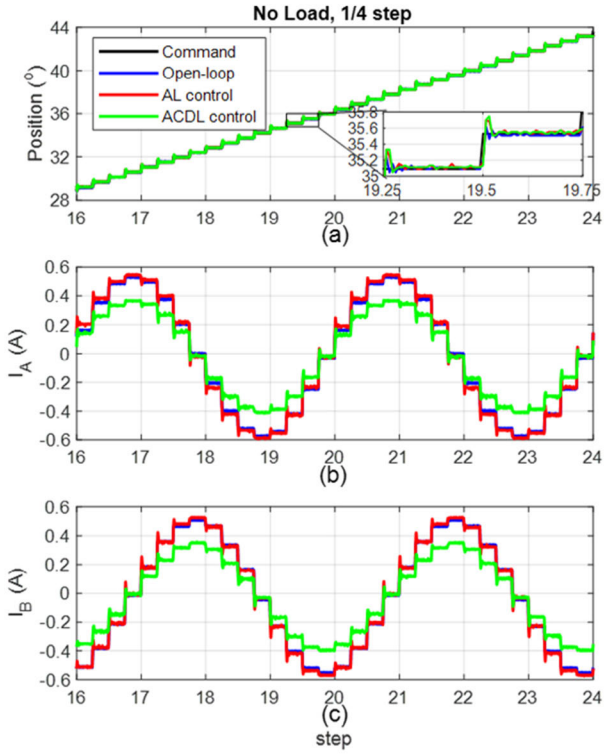

FIGURE 16. Data obtained under the no-load condition with a 1/4 microstep drive for eight steps.

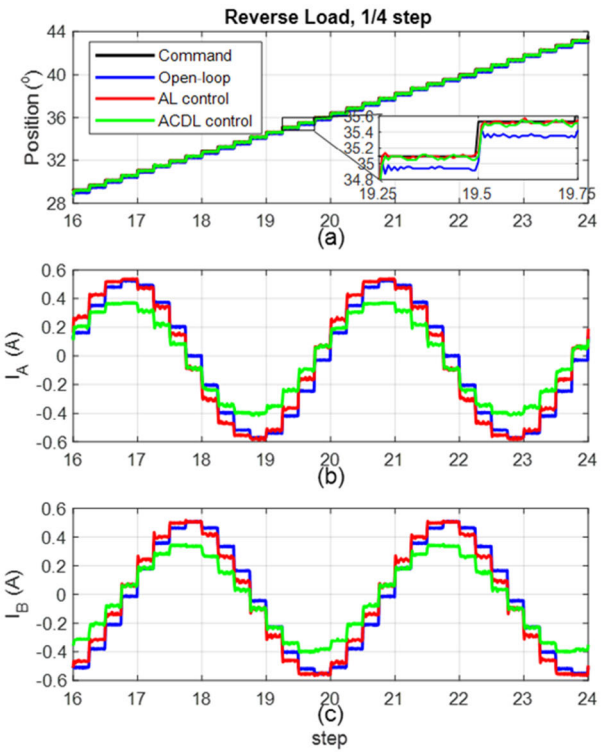

FIGURE 17. Data obtained under the reverse-load condition with a 1/4 microstep drive for eight steps.

The impact of stepping can be reduced by reducing the angle of each advance through a microstepping drive. Fig. 16 shows the data obtained under the no-load condition for eight full steps when a 1/4-step advance occurred in each of the 32 microsteps. The enlarged view of the rotor angle curve in Fig. 16(a) indicates that 1/4 microstepping led to a smaller overshoot angle compared with that observed under full stepping. Under open-loop control, a steady state was reached with a small error from the command angle (as with a full-step drive). Fig. 16(b) and 16(c) depict the current curves for phases A and B, respectively. The current waveforms of the three control methods are similar to sine and cosine waves. When no load existed, no obvious difference existed in the phases of the three control methods; however, the amplitude controlled through ACDL was clearly lower than those controlled through the other two control methods. In AL control and ACDL control, because angular error feedback affected the excitation angle and current distribution, the two-phase currents exhibited a transient overshoot in the beginning of phase switching and then quickly converged to a steady state.

Fig. 17 displays the data obtained under the reverse-load condition for eight full steps when a 1/4-step advance occurred in each of the 32 microsteps. The enlarged part of the rotor angle change curve in Fig. 17(a) indicates that the reverse-load condition resulted in the open-loop control process being unable to catch up with the command step and that the AL and ACDL control methods reduced the angular error. Fig. 17(b) and 17(c) display the current curves for phases A and B, respectively, under the aforementioned conditions. The sine-wave phase of the open-loop control mode was similar under the no-load and reverse-load conditions. The phase of the current sine wave in AL control advanced to offset the rotation-phase lag caused by the reverse load. In ACDL control, the current amplitude decreased because phase d was suppressed, and the phase advance was greater than that in AL control.

Fig. 18 depicts the data obtained under the reverse-load condition for eight full steps when a 1/4-step advance occurred in each of the 32 microsteps under the forward-load condition. The enlarged part of the rotor angle change curve in Fig. 18(a) indicates that the forward-load condition resulted in a leading angular error in the open-loop control method and that the AL and ACDL control methods reduced this angular error. Fig. 18(b) and 18(c) display the current curves for phases A and B, respectively, under the aforementioned conditions. The phase of the sine wave in the open-loop control mode did not differ considerably between the forward-load and no-load conditions. In the AL control method, the phase of the current sine wave lags behind that in the open-loop control method, which offsets the phase advance caused by the forward load. In the ACDL control method, the amplitude decreased because phase d was suppressed, and the phase lagged to a greater extent than in the open-loop control method.

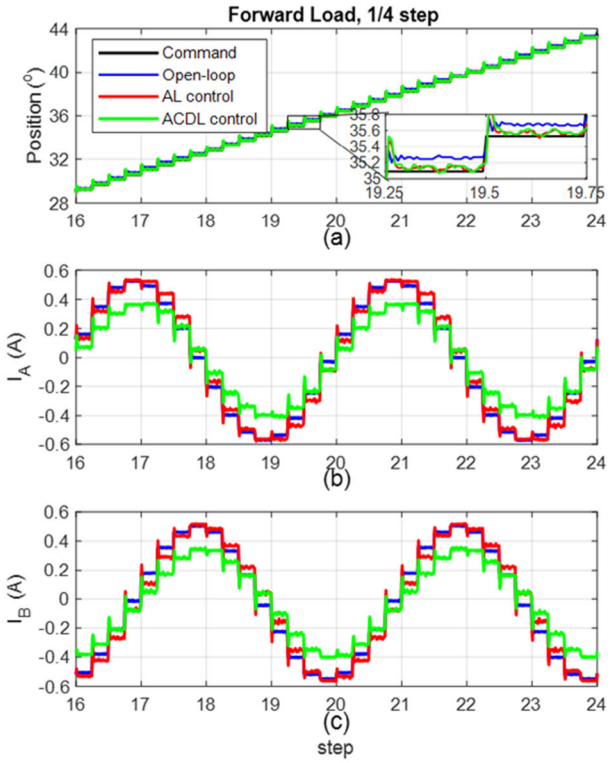

FIGURE 18. Data obtained under the forward-load condition with a 1/4 microstep drive for eight steps.

TABLE 2. Experimental values of the average angular error, the standard deviation of the angular error, and the power consumption in the three control methods.

Data (unit)	load / Method	1 step			1/2 step			1/4 step			1/8 step		
		0g	-20g	+20g	0g	-20g	+20g	0g	-20g	+20g	0g	-20g	+20g
$Error_{RMS}$ (°)	Open loop	0.044	0.184	0.166	0.049	0.194	0.161	0.056	0.207	0.149	0.061	0.215	0.136
	AL control	0.021	0.029	0.039	0.022	0.026	0.041	0.019	0.031	0.032	0.019	0.033	0.031
	ACDL control	0.024	0.039	0.050	0.021	0.028	0.038	0.023	0.041	0.042	0.023	0.056	0.041
$Error_{STD}$ (°)	Open loop	0.024	0.038	0.044	0.025	0.043	0.046	0.031	0.043	0.046	0.034	0.043	0.046
	AL control	0.006	0.011	0.011	0.006	0.010	0.010	0.006	0.009	0.009	0.006	0.011	0.011
	ACDL control	0.007	0.012	0.011	0.007	0.012	0.011	0.007	0.010	0.010	0.008	0.024	0.013
Power (W)	Open loop	1.848	1.869	1.906	1.845	1.823	1.815	1.831	1.818	1.806	1.916	1.873	1.851
	AL control	1.993	1.946	1.919	1.950	1.911	1.844	1.921	1.885	1.855	1.831	1.854	1.833
	ACDL control	0.991	0.992	0.971	0.961	0.971	0.939	0.908	0.917	0.916	0.928	0.943	0.924

The results obtained for 1/2 and 1/8 microstepping were the same as those obtained for full stepping and 1/4 microstepping. The experimental data obtained for the aforementioned microstepping conditions are displayed in Fig. 19. Moreover, Table 2 presents the experimental values of the average angular error, the standard deviation of the angular error, and the power consumption in the three control methods.

Fig. 19(a)–19(d) show the root mean square (RMS) angular error in the three control methods, and these values represent the steady-state positioning accuracy of the control methods. Irrespective of the number of microsteps, the maximum error (approximately 0.2°) in the open-loop control method occurred under reverse load. Moreover, the maximum errors under forward load and no load were approximately 0.15° and 0.05°, respectively. Irrespective of the load, in the AL and ACDL control methods, the RMS error was smaller than 0.05°, which corresponded to approximately 2–3 encoder

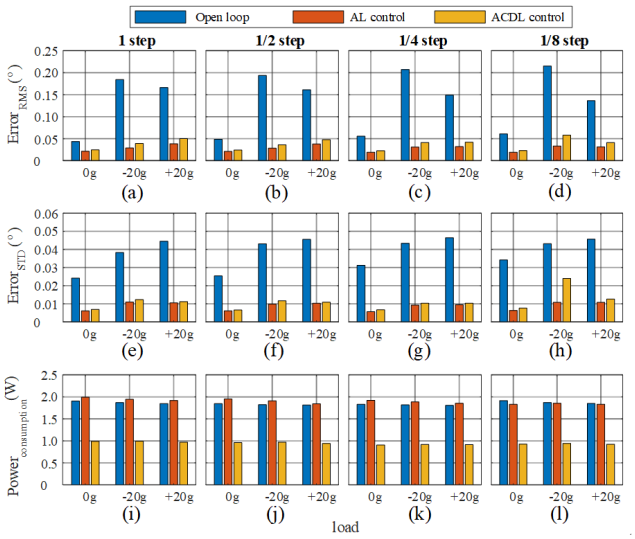

FIGURE 19. Bar graphs of the experimental values of the average angular error, the standard deviation of the angular error, and the power consumption in the three control methods. (a)–(d) RMS values of the angular error, which represent the steady-state positioning accuracy. (e)–(h) Standard deviations of the angular error, which represent the strength of oscillations at the target position. (i)–(l) Average power consumption, which represents energy efficiency.

counts. Compared with AL control, ACDL control consumed less power but was less accurate.

Fig. 19(e)–19(h) display the standard deviations of the angular error, which represent the strength of the oscillations during stable positioning. These figure parts indicate that irrespective of the number of microsteps, the influence of load on stability was not obvious. Of the three control methods, the open-loop control method was the most unstable, whereas the AL control method was the most stable.

Fig. 19(i)–19(l) present the average power consumption for the three control methods. Regardless of the number of microsteps or the type of load, the power consumption remained the same in the open-loop and AL control methods, as the total current was fixed. In the ACDL control method, the rated and minimum currents are used as the upper and lower current limits, respectively; thus, the current was adjusted according to the acceleration and load of the motor, and the power consumption is inevitably lower in ACDL control than in the other two control methods. Reverse load requires the motor to do additional work to turn the rotor; forward load can pull the rotor until it reaches the target point. Thus, the motor does not need additional power consumption. However, because the experimental speed was extremely low, the rotor remained stationary most of the time, and the power consumed during rotation was negligible.

VI. CONCLUSION

In this paper, an innovative method, namely ACDL control, is proposed for stepping motor drive control. The proposed method can increase positioning accuracy while decreasing power consumption. In this study, the proposed method

was tested by implementing it using a driving system. The results obtained with the proposed method were compared with those obtained using the open-loop and AL control methods.

To verify the effectiveness of the constructed motor driver, a test platform that could apply forward and reverse loads was constructed, and experiments were performed by implementing the open-loop, AL, and ACDL control methods on this platform. The experiments were conducted under full-step operation, 1/2 microstepping, 1/4 microstepping, and 1/8 microstepping in the no-, forward-, and reverse-load conditions.

The experimental data indicated that AL control can improve the anti-load capacity of a traditional open-loop microstepping drive and increase its positioning accuracy by 472%. ACDL control can reduce power consumption by 48.8% while improving accuracy. For the 14-bit angle encoder used in the experiments, the final positioning accuracy was 2–3 encoder counts, which corresponded to approximately 0.05°.

REFERENCES

[1] M. Zou, J. Yu, Y. Ma, L. Zhao, and C. Lin, "Command filtering-based adaptive fuzzy control for permanent magnet synchronous motors with full-state constraints," *Inf. Sci.*, vol. 518, pp. 1–12, May 2020.

[2] Q. Wei, X.-Y. Wang, and X.-P. Hu, "Optimal control for permanent magnet synchronous motor," *J. Vib. Control*, vol. 20, no. 8, pp. 1176–1184, 2014.

[3] H. Hagino and K. Igeta, "Jikken de Manabu DC mota no Maikon-Seigyojutsu," Shikyushuppan, Japan, Tech. Rep., Jul. 2012.

[4] Z. A. Barabas and A. Morar, "High performance microstepping driver system based on five-phase stepper motor (sine wave drive)," *Proc. Technol.*, vol. 12, pp. 90–97, Jan. 2014, doi: 10.1016/j.protcy.2013.12.460.

[5] Z. Q. Zhu, J. T. Chen, L. J. Wu, and D. Howe, "Influence of stator asymmetry on cogging torque of permanent magnet brushless machines," *IEEE Trans. Magn.*, vol. 44, no. 11, pp. 3851–3854, Nov. 2008, doi: 10.1109/TMAG.2008.2001322.

[6] Z. Q. Zhu, "A simple method for measuring cogging torque in permanent magnet machines," in *Proc. IEEE Power Energy Soc. Gen. Meeting*, Jul. 2009, pp. 1–4, doi: 10.1109/PES.2009.5275665.

[7] S. Nian, L. Zhu, X. Luo, and Z. Huang, "Analytical methods for optimal rotor step-skewing to minimize cogging torque in permanent magnet motors," in *Proc. 22nd Int. Conf. Electr. Mach. Syst. (ICEMS)*, Aug. 2019, pp. 1–5, doi: 10.1109/ICEMS.2019.8921502.

[8] S. Derammelaere, B. Vervisch, F. De Belie, B. Vanwalleghem, J. Cottyn, P. Cox, G. Van den Abeele, K. Stockman, and L. Vandevelde, "The efficiency of hybrid stepping motors: Analyzing the impact of control algorithms," *IEEE Ind. Appl. Mag.*, vol. 20, no. 4, pp. 50–60, Jul. 2014, doi: 10.1109/MIAS.2013.2288403.

[9] M. Bodson, J. N. Chiasson, R. T. Novotnak, and R. B. Rekowski, "High-performance nonlinear feedback control of a permanent magnet stepper motor," *IEEE Trans. Control Syst. Technol.*, vol. 1, no. 1, pp. 5–14, Mar. 1993, doi: 10.1109/87.221347.

[10] M. Cheles. *Sensorless Field Oriented Control (FOC) for a Permanent Magnet Synchronous Motor (PMSM) Using a PLL Estimator and Field Weakening (FW)*. Accessed: Apr. 21, 2023. [Online]. Available: https://www.microchip.com/en-us/application-notes/an1292

[11] W. H. Yeadon and A. W. Yeadon, *Handbook of Small Electric Motors*. New York, NY, USA: McGraw-Hill, 2001.

[12] D.-H. Lee, W. Che, and J.-W. Ahn, "Micro-step position control with a simple voltage controller using low-cost micro-processor," in *Proc. IEEE Int. Symp. Ind. Electron.*, Jul. 2010, pp. 1378–1382, doi: 10.1109/ISIE.2010.5637223.

[13] S. Kim and C. K. Ahn, "Variable-performance positioning law for hybrid-type stepper motors via active damping injection and disturbance observer," *IEEE Trans. Circuits Syst. II, Exp. Briefs*, vol. 68, no. 4, pp. 1308–1312, Apr. 2021, doi: 10.1109/TCSII.2020.3020224.

[14] Q. Ni, M. Yang, S. A. Odhano, M. Tang, P. Zanchetta, X. Liu, and D. Xu, "A new position and speed estimation scheme for position control of PMSM drives using low-resolution position sensors," *IEEE Trans. Ind. Appl.*, vol. 55, no. 4, pp. 3747–3758, Jul. 2019, doi: 10.1109/TIA.2019.2904934.

[15] S. H. Noh and K. H. Kim, "A study on closed-loop control of a stepping motor for resonance elimination," *J. Korean Soc. Mech. Eng.*, vol. 15, no. 1, pp. 90–97, 1991.

[16] C. Zhou and B. Liu, "A hybrid stepper motor control solution based on a low-cost position sensor," in *Proc. IEEE Int. Conf. Mechatronics Autom. (ICMA)*, Aug. 2019, pp. 1836–1841, doi: 10.1109/ICMA.2019.8816190.

[17] F. Bernardi, E. Carfagna, G. Migliazza, G. Buticchi, F. Immovilli, and E. Lorenzani, "Performance analysis of current control strategies for hybrid stepper motors," *IEEE Open J. Ind. Electron. Soc.*, vol. 3, pp. 460–472, 2022, doi: 10.1109/OJIES.2022.3185659.

[18] K. M. Le, H. Van Hoang, and J. W. Jeon, "An advanced closed-loop control to improve the performance of hybrid stepper motors," *IEEE Trans. Power Electron.*, vol. 32, no. 9, pp. 7244–7255, Sep. 2017, doi: 10.1109/TPEL.2016.2623341.

[19] T. Kenjo, *Stepping Motors and Their Microprocessor Controls Monographs in Electrical and Electronic Engineering*. Oxford, U.K.: Oxford Univ., 1984, pp. 25–49.

[20] W. D. Jones, "Control of stepping motors—A tutorial," Univ. Iowa. Accessed: Jan. 13, 2023. [Online]. Available: http://homepage.divms.uiowa.edu/~jones/step/

[21] A. Arias, J. Caum, E. Ibarra, and R. Griñó, "Reducing the cogging torque effects in hybrid stepper machines by means of resonant controllers," *IEEE Trans. Ind. Electron.*, vol. 66, no. 4, pp. 2603–2612, Apr. 2019, doi: 10.1109/TIE.2018.2844786.

[22] M. Bodson, J. S. Sato, and S. R. Silver, "Spontaneous speed reversals in stepper motors," *IEEE Trans. Control Syst. Technol.*, vol. 14, no. 2, pp. 369–373, Mar. 2006, doi: 10.1109/TCST.2005.863675.

[23] K. W.-H. Tsui, N. C. Cheung, and K. C.-W. Yuen, "Novel modeling and damping technique for hybrid stepper motor," *IEEE Trans. Ind. Electron.*, vol. 56, no. 1, pp. 202–211, Jan. 2009, doi: 10.1109/TIE.2008.2008791.

[24] Y. W. Jeong, Y. Lee, and C. C. Chung, "A survey of advanced control methods for permanent magnet stepper motors," *J. Mar. Sci. Technol.*, vol. 28, no. 5, pp. 331–342, Mar. 2020, doi: 10.6119/JMST.202010_28(5).0002.

[25] Sheng Fu Machinery CO., LTD. *2020_Stepper_Catalogue*. Accessed: Apr. 21, 2023. [Online]. Available: https://www.sumfu.com/

SHYH-BIAU JIANG (Member, IEEE) received the B.S. degree in agricultural machinery engineering from National Taiwan University, Taipei City, Taiwan, in 1982, the M.S. degree in power mechanical engineering from National Tsing Hua University, Hsinchu, Taiwan, in 1984, and the Ph.D. degree in mechanical engineering from the University of California at Los Angeles, Los Angeles, CA, USA, in 1992.

He is currently a Professor with the Institute of Optical-Mechatronics Engineering and the Department of Mechanical Engineering, National Central University, Taoyuan, Taiwan. He has helped his previous Ph.D. and M.S. students to establish a company to commercialize their technology in automation. He is the holder of over 20 patents. His current research interest includes the development of digitized measuring instruments.

HSIANG-CHUN CHUANG received the master's degree in mechanical engineering from the National Taiwan University of Science and Technology, Taipei, Taiwan, in 2012. He is currently pursuing the Ph.D. degree with the Institute of Optical-Mechatronics Engineering, National Central University, Taoyuan, Taiwan. He is a Research and Development Engineer with the National Chung-Shan Institute of Science and Technology, Taoyuan, specializing in missile guidance, trajectory simulation, and system engineering. His current research interests include microcontrollers, sensor calibration, and motor drives.

CHUNG-WEI KUNG received the master's degree from the Institute of Optical-Mechatronics Engineering, National Central University, Taoyuan, Taiwan, in 2022. His research interests include microcontrollers, encoder calibration, and the closed-loop control of microstepping motors.

XIANG-GUAN DENG received the master's degree from the Institute of Optical-Mechatronics Engineering, National Central University, Taoyuan, Taiwan, in 2020. During his studies, he mainly studied embedded systems, including microcontrollers, sensor drivers, circuit board design, and motor control. After completing his master's degree, he began working as a Firmware Engineer at IC design company mainly designing industrial control and automotive MCUs, and researching how to implement functional safety with software or hardware technology.

YEN-PING SHEN received the master's degree from the Institute of Optical-Mechatronics Engineering, National Central University, Taoyuan, Taiwan, in 2021. Since his studies, he has specialized in developing software and firmware for microcontrollers. He is also good at hardware development and is familiar with the development process of microcontrollers, including Bluetooth controllers with the Internet of Things functions, switching power supply modules, and microstepping motor driver boards. He worked at Taiwan Semiconductor Manufacturing Company after completing his master's degree.

LI-WU CHEN received the Ph.D. degree from National Central University, Taoyuan, Taiwan, in 2021. His specialty is opto-mechatronics integration engineering, including electric control, firmware design, hardware design, mechanism design, and algorithm implementation on the microcontroller. His research interest includes the development and calibration test of an innovative airglow instrument for space weather science payloads.